

ATLAS BASED 3D LIVER SEGMENTATION USING ADAPTIVE THRESHOLDING AND SUPERPIXEL APPROACHES

Negar Farzaneh^{1,2}, Samuel Habbo-Gavin³, S.M.Reza Soroushmehr^{2,4}, Hirenkumar Patel³,
David P. Fessell⁵, Kevin R. Ward^{2,4}, Kayvan Najarian^{1,2,4}

¹ Department of Computational Medicine and Bioinformatics,

² Michigan Center for Integrative Research in Critical Care (MCIRCC),

³ Department of Computer Science, ⁴ Department of Emergency Medicine, ⁵ Department of Radiology,
University of Michigan, Ann Arbor, MI, USA

ABSTRACT

Traumas and illnesses can cause injury in internal organs. The liver, being the largest abdominal organ, is most likely to be injured by trauma. Currently CT scans are analyzed by radiologists to see if there is any injuries in organs; however, due to the large amounts of data and its complexity in terms of noise, intensity variations in different images and so on, visual inspection would be time consuming and prone of error. Therefore, an automated approach would be beneficial. In this paper we propose a fully automated Bayesian based method for 3D segmentation of the liver. Experimental results show that the proposed method can achieve high performance with Dice and Jaccard similarity coefficients of 93.5% and 87.9% respectively.

keywords - Image segmentation, Abdominal injuries, Liver segmentation, Probabilistic atlas, Adaptive threshold, Superpixel.

1. INTRODUCTION

Traumatic injury is the leading cause of death among Americans younger than 46 [1]. Traumatic pelvic and abdominal injuries are among the most severe types of trauma. Clinical signs alone are not sufficient to make diagnosis of stable abdominal injuries and missed injuries are a common cause of morbidity and late mortality [2]. In order to assess stable abdominal trauma patients, Computed Tomography (CT) is used which is the most widely imaging modality considered as a gold standard source of imaging [3].

At this point two issues need to be addressed in case of trauma patients. First, determining accurate diagnosis based on generated data that is of a crucial importance to prevent further injuries and make efficient treatment plans. Second, traditional inspection of the large volume of different varieties of data for each trauma patient is both time consuming and prone to human error. In current practice, CT scans

are visually inspected, whereas their size and complexity adversely affect the reliability. A computer-assisted support decision system capable of rapidly analyzing large volumes of patient information to generate accurate diagnosis and prognosis has the potential to improve both patient care/survival and resource utilization. Today, image segmentation is a mature field in medical image processing and provides physicians with (semi-)automated computer-aided assistance.

Liver, due to its size and position, is the most vulnerable abdominal organ [4]. In addition, since large blood vessels are embedded in liver, its injuries cause serious risk for complications such as shock, so liver inspection is of a high priority. Following the aforementioned need, an automated method of liver segmentation is proposed in this paper.

Through the past decade we have gone through major advancement in the field of (semi-)automated liver segmentation, though it is still a challenging problem. Lue *et al.* [5] reviewed different methods on automated liver segmentation. Some previously proposed methods for liver segmentation include Semi-automatic and automatic algorithm based on deformable model [6], statistical shape model (SSM) [7, 8] and probabilistic atlas (PA) [9].

In this paper we propose a method for segmenting the liver in abdominopelvic traumatic injured patients. We assume that the liver has similar geometric structure as well as position among different patients. Our method employs probabilistic atlases (PA) for both location and intensity of liver.

We first register annotated images (i.e. images with manually annotations for liver) and then create a Bayesian probability model that accounts for location and intensity. A thresholded result is then adapted using further anatomical information and given to the final stage of the process. The final stage uses a clustering method based on a superpixel approach [10]. The segmentation is completed by applying post-processing to the result of the thresholded superpixels.

The remainder of this paper is organized as follows. In section 2 we discuss our previous work, and in section 3 cur-

rent modifications are outlined. In section 4, more details of the proposed adaptive thresholding technique are discussed, followed by the improvement of the region of interest (ROI) in section 5. Section 6 discusses the application of superpixels in generating the final segmentation. Finally, section 7 presents the experimental results and concludes the paper.

2. RELATED WORKS ON LIVER SEGMENTATION

In our previous work [11], we proposed a Bayesian based method for segmenting the liver. The method involved first normalizing the abdominal cavity of each patient’s CT scan. Two atlases were then created using 8 patients’ sets of CT scans. The first atlas was based on liver location in the abdomen and was generated by calculating the probability of each pixel belonging to the liver. The second atlas was generated by calculating the probability of a pixel being liver given its intensity. Given a new set of slices, for each input pixel the location probability, $P(L|(i, j))$, and intensity probability, $P(L|I)$, of that pixel is calculated based on its coordinates (i, j) and intensity I . Then the overall probability of that pixel being liver is defined as:

$$P(L|(i, j), I) = \frac{P(I, (i, j)|L)P(L)}{P(I, (i, j)|L)P(L) + P(I, (i, j)|L')P(L')} \quad (1)$$

By considering $P(L) \approx P(L')$, $P(L|I) \propto P(I|L)$, and $P(L|(i, j)) \propto P((i, j)|L)$ since intensity and position are two independent random variables, we conclude that:

$$P(L|(i, j), I) \propto P(L|I)P(L|i, j) \quad (2)$$

By applying a predefined threshold on the mentioned probability values, an approximate of the liver position/intensity is acquired. In the next step, by having the rough approximation, a customized and more accurate new intensity probability atlas, $P(I|L)_{new}$, is build. The new probability of a pixel being the liver is calculated as:

$$P_{new}(L|I, (i, j)) \propto P(L|I)_{new}P(L|i, j) \quad (3)$$

An initial segmentation for each slice was generated using a fixed-threshold to separate liver pixels from background. After that, a post-processing approach was carried out to refine the segmentation. Although this method achieves high performance in terms of sensitivity and specificity, it has a drawback in distinguishing the border between liver and other organs/tissue. In the next section we propose a method to further improve this method.

3. PROPOSED IMPROVEMENTS

This paper will improve upon the methods proposed in [11]. The first improvement is to replace the constant threshold of

liver probability with an adaptive one. The result of an adaptive thresholding will then be used as an original ROI for the next stage. The region will be modified automatically using generalized anatomical information. This final ROI will be used in connection with superpixels to achieve a final segmentation. The flowchart in Figure 1 shows the stages in the segmentation process.

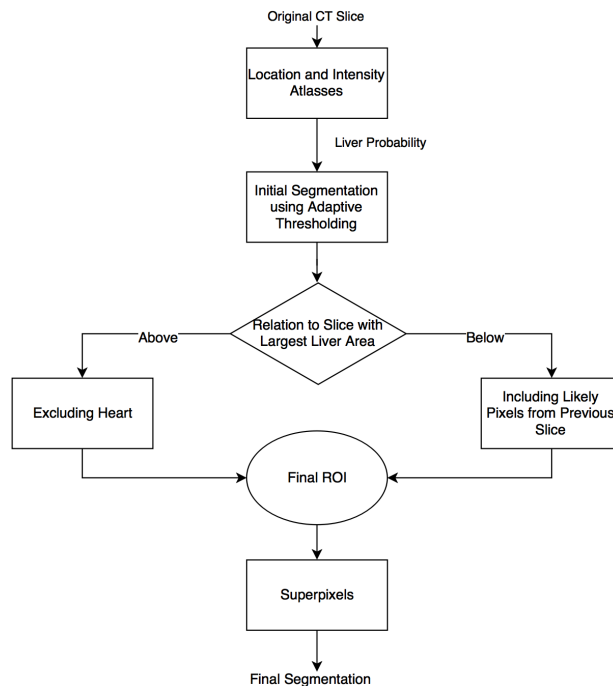


Fig. 1: Flowchart of the proposed liver segmentation method

4. ADAPTIVE THRESHOLDING

In the previous work after calculating the probability of each pixel being liver based on its coordinates and intensity (i.e. Eq (3)), a fixed threshold was used as a cutoff value to segment the liver. In this paper, we propose an adaptive threshold for each single slice of each patient. To calculate the threshold, probability values for pixels of that slice are normalized first and then for all values of an acceptable range of cutoff probabilities, which are heuristically determined to be in the range of t_1 to t_2 with the step size of Δ , the segmented liver is acquired by applying each of the t_i thresholds. It is obvious that a set of pixels detected as liver by a cutoff value of t , is a subset of pixels resulted from a lower threshold. We found out that at the optimum threshold, th , the segmentation reaches a stable state which means that it has the minimum changes when the threshold is increased by Δ . Therefore, the optimum cutoff value of t is calculated by:

$$f(t) = \frac{\|P_{new}^{\geq t-\Delta}\|_0 - \|P_{new}^{\geq t}\|_0}{\|P_{new}^{\geq t}\|_0}$$

$$th = \arg \min_{t_1 \leq t \leq t_2} f(t) \quad (4)$$

where $P_{new}^{\geq t}$ is a binary image with the pixel value of 1 when the corresponding pixel in P_{new} is greater than or equal to t . Also, $\|\cdot\|_0$ denotes the norm zero. At the next step, post-processing including filling the holes, removing small objects and smoothing the 3D component is applied.

The result of the segmentation after applying adaptive thresholding compared to the segmentation with a constant threshold is shown in section 7.

5. GENERATING THE NEW ROI

The liver segmentation improvement is accomplished in two stages. First, the anatomical information is incorporated into the approximate region of liver generated by adaptive thresholding to create a new ROI. Then the liver is segmented using the ROI and the application of superpixels.

Before anatomical information can be incorporated, it is necessary to find a slice at which the liver appears largest. This is assumed to be the slice with the maximum area in the approximated liver region. The area of liver is growing until reaching this slice and after that it gets smaller. Knowing this, a different method is applied to each side of the division.

5.1. Slices with Increasing Liver Area

In slices above the one with the liver appears largest, the nearby abdominal cavity does not usually contain objects of similar appearance except for the heart. Figure 2a shows that the heart is nearly indistinguishable from the liver and thus anatomical information should be used to assist the segmentation.

The heart begins higher in the body than the liver and therefore it is visible sooner than the liver and fades out to make room for the liver. The heart also has a slightly higher intensity due to the contrast dye in the blood.

In order to generate the new ROI, Figure 2b is created. Note that the area in the red box shows the heart. Figure 2b is generated by subtracting the current slice from its upper slice. Figure 2b appears bright where slice n is darker than slice $n - 1$, signifying that the region may be the heart. Now, dark regions, e.g. in the green box in Figure 2b, show liver growth into previously unoccupied space. Bright regions, e.g. in the red box, show where the intensity is decreasing, the signature of the heart beginning to fade.

Figure 2b is then thresholded to exclude the heart. The change in the ROI is shown in Figure 2c. The gray region was removed using the anatomical information. Figure 2d shows the improvement in the final result.

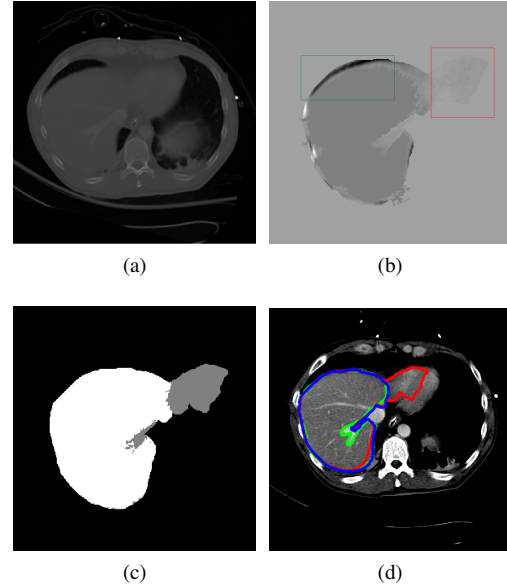


Fig. 2: Improving ROI for slices before the largest liver area. (a): Original image (b): Intensity change from previous slice: Bright pixels represent decreasing intensity from previous slice. (c): Change in ROI: gray was removed (d): Improvement in final segmentation displayed on adjusted image. The green is ground truth, red is the approximate, and blue is the final result. The final result line overlays some other regions.

5.2. Slices with Decreasing Liver Area

In the slices below the one where the liver appears largest, the nearby abdominal cavity often contains other objects which might have similar appearance to the liver. Additionally in one slice, the liver may appear as two or more disjoint components. The new ROI starts with dilating the segmentation result of the adaptive thresholding approach. This part of the ROI is visible in Figure 3a as the white region. By assuming that this might be an underestimate, we look at the result of the one above slice, L_{n-1} . P_n corresponds to 2D matrix of P_{new} values of slice n . $I(B)$ corresponds to a set of pixels' intensity from the original image masked by B . New pixels are added to the segmentation by using:

$$ROI_n = L_{n-1} \cap \text{dilate}(P_n^{\geq th}) \quad (5)$$

$$\text{Added} = \left\{ q \in ROI_n \mid \left| I(q) - \mu(I(P_n^{\geq th})) \right| < 0.5 \sigma(I(P_n^{\geq th})) \right\}$$

These pixels, still considered likely to be liver, are gray in Figure 3a. Figure 3b shows the improvement in the final result from the approximate ROI.

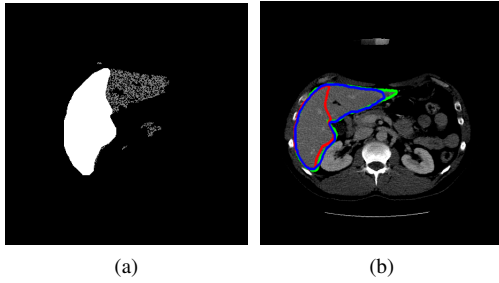


Fig. 3: Improving ROI for slices after largest liver area. (a): Change in ROI: gray was added (b): Improvement in final segmentation displayed on adjusted image. The green is ground truth, red is the approximate ROI, and blue is the final result. The final result overlays some parts of other borders.

6. CONSTRUCTING THE FINAL SEGMENTATION USING SUPERPIXEL

The ROI calculated in the previous section is an approximate of the liver which included a basic dilation. In different locations it may be an under or overestimate. Simple thresholding could create issues such as including parts of nearby structures. To resolve this issue, superpixel approach is used that incorporates more information into the decision. The superpixels were generated using *Simple Linear Iterative Clustering* (SLIC)[12]. SLIC clusters the image through k-means considering both intensity and location coordinates. The set of all superpixels is S .

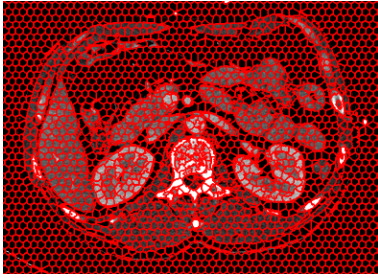


Fig. 4: Contrast adjusted image with superpixel boundaries.

A list of all superpixels that have intersection with the ROI is then generated.

$$L_s = \{s_i \in S \mid s_i \cap ROI \neq \phi\} \quad (6)$$

The liver statistics are described for each slice using the mean and standard deviation of the approximate segmentation. The mean of each superpixel on the list is calculated. A superpixel is then added to the final segmentation if the superpixels mean is within 1.5 standard deviations of the mean of the input segmentation.

$$L_n = \{s_i \in L_s \mid |\mu(s_i) - \mu(I(P_n^{\geq th}))| < 1.5 \sigma(I(P_n^{\geq th}))\} \quad (7)$$

Superpixels provide two major advantages over thresholding. First, by analyzing clusters, the inclusion into the segmentation represents an object rather than a dash of ideal pixels. This is crucial as post-processing fills holes in the final segmentation. Second, superpixels provide a way to include pixels that are near the ROI as long as they are part of a cluster that has intersection with the region.

7. EXPERIMENTAL RESULTS AND CONCLUSION

8 patients with total of 332 CT images are used to create two atlases. The algorithm is tested on 503 slices from 10 patients, 7 sets are from University of Michigan Hospital and 3 from Virginia Commonwealth University Hospital. The results of segmentation are generated at three different stages. 1) Previously published algorithm which used constant cutoff value. 2) Applying an adaptive cutoff value, 3) Final results after implementing anatomical information and superpixels for refinement of results from stage 2. The results of these three different stages are compared to ground truth validated by a radiologist. Voxel-wise Dice, Jaccard, sensitivity, and specificity similarity values are calculated to evaluate the proposed segmentation methods. The average of these four coefficient is calculated over 10 subjects in the test data set and reported in Table 1. As shown in Table 1 all coefficients are improved except for specificity which stays the same. The final Dice and Jaccard values are 93.5% and 87.9% respectively. Two similar approaches that used atlases achieved Dice values of 94%[13] and 95.1%[14]. The Dice value of a superpixel based method was 94.1% [10]. Our algorithm, unlike the mentioned methods, was developed and tested on CT images of traumatic abdominal and pelvic patients. These images have a lot of variations, and we only used 8 images to create the atlases. Therefore, the atlases do not capture the full variability.

Table 1: Results of proposed method at different stages of the algorithm, each coefficient is acquired by the average of the corresponding coefficient over all 10 subjects in the test data set.

Segmentation result	Previous approach	Adaptive threshold	Final segmentation
Dice	88.3%	90.7%	93.5%
Jaccard	79.3%	83.1%	87.9%
Sensitivity	81.7%	85.3%	90.6%
Specificity	99.5%	99.6%	99.5%

8. ACKNOWLEDGMENT

This material is based upon work supported by the National Science Foundation under Grant No. 1500124.

9. REFERENCES

- [1] P. Rhee, B. Joseph, V. Pandit, H. Aziz, G. Vercruyssen, N. Kulvatunyou, and R. Friese, "Increasing trauma deaths in the united states," *Annals of surgery*, vol. 260, no. 1, pp. 13–21, 2014.
- [2] J. Jansen, S. Yule, and M. Loudon, "Investigation of blunt abdominal trauma," *British Medical Journal*, vol. 7650, pp. 938, 2008.
- [3] F. Abu-Zidan, M. Sheikh, F. Jadallah, and J. Windsor, "Blunt abdominal trauma: comparison of ultrasonography and computed tomography in a district general hospital," *Australasian radiology*, vol. 43, no. 4, pp. 440–443, 1999.
- [4] T. Fabian and T. Bee, "Liver and biliary tract trauma," *Trauma. 5th ed. New York, NY: McGraw-Hill*, pp. 637–662, 2003.
- [5] S. Luo, X. Li, and J. Li, "Review on the methods of automatic liver segmentation from abdominal images," *Journal of Computer and Communications*, vol. 2, no. 02, pp. 1, 2014.
- [6] J. Lu, L. Shi, M. Deng, C. Simon, and P. Heng, "An interactive approach to liver segmentation in ct based on deformable model integrated with attractor force," in *Machine Learning and Cybernetics (ICMLC), 2011 International Conference on*. IEEE, 2011, vol. 4, pp. 1660–1665.
- [7] X. Zhang, J. Tian, K. Deng, Y. Wu, and X. Li, "Automatic liver segmentation using a statistical shape model with optimal surface detection," *Biomedical Engineering, IEEE Transactions on*, vol. 57, no. 10, pp. 2622–2626, 2010.
- [8] M. Erdt, S. Steger, M. Kirschner, and S. Wesarg, "Fast automatic liver segmentation combining learned shape priors with observed shape deviation," in *Computer-Based Medical Systems (CBMS), 2010 IEEE 23rd International Symposium on*. IEEE, 2010, pp. 249–254.
- [9] H. Park, P. Bland, and C. Meyer, "Construction of an abdominal probabilistic atlas and its application in segmentation," *Medical Imaging, IEEE Transactions on*, vol. 22, no. 4, pp. 483–492, 2003.
- [10] T. Kitrungsakul, X. Han, and Y. Chen, "Liver segmentation using superpixel-based graph cuts and restricted regions of shape constrains," *IEEE International Conference on Image Processing (ICIP)*, 2015.
- [11] N. Farzaneh, S. Samavi, S.M.R. Soroushmehr, H. Patel, S. Habbo-Gavin, D. Fessell, K. Ward, and K. Najarian, "Liver segmentation using location and intensity probabilistic atlases," in *International Conference of the IEEE Engineering in Medicine and Biology Society (EMBC)*. IEEE, 2016.
- [12] R. Achanta, A. Shaji, K. Smith, A. Lucchi, P. Fua, and S. Süsstrunk, "Slic superpixels compared to state-of-the-art superpixel methods," *IEEE transactions on pattern analysis and machine intelligence*, vol. 34, no. 11, pp. 2274–2282, 2012.
- [13] R. Wolz, C. Chu, K. Misawa, K. Mori, and D. Rueckert, "Multi-organ abdominal ct segmentation using hierarchically weighted subject-specific atlases," *MICCAI*, vol. 7510, pp. 10–17, 2012.
- [14] C. Chu, M. Oda, T. Kitasaka, K. Misawa, M. Fujiwara, Y. Hayashi, Y. Nimura, D. Rueckert, and K. Mori, "Multi-organ segmentation based on spatially-divided probabilistic atlas from 3d abdominal ct images," *MICCAI*, vol. 8150, pp. 165–172, 2013.